



Twin Meander Coil: Sensitive Readout of Battery-free On-body Wireless Sensors Using Body-scale Meander Coils

RYO TAKAHASHI, The University of Tokyo, Japan
WAKAKO YUKITA, The University of Tokyo, Japan
TAKUYA SASATANI, The University of Tokyo, Japan
TOMOYUKI YOKOTA, The University of Tokyo, Japan
TAKAO SOMEYA, The University of Tokyo, Japan
YOSHIHIRO KAWAHARA, The University of Tokyo, Japan



Fig. 1. Twin Meander Coil is fabricated on garments using industrial knitting machines and can wirelessly read out on-body battery-free sensors placed throughout the garment surface.

Energy-efficient and unconstrained wearable sensing platforms are essential for ubiquitous healthcare and activity monitoring applications. This paper presents Twin Meander Coil for wirelessly connecting battery-free on-body sensors to a textile-based reader knitted into clothing. This connection is based on passive inductive telemetry (PIT), wherein an external reader coil collects data from passive sensor coils via the magnetic field. In contrast to standard active sensing techniques, PIT does not require the reader to power up the sensors. Thus, the reader can be fabricated using a lossy conductive thread and industrial knitting machines. Furthermore, the sensors can superimpose information such as ID, touch, rotation, and pressure on its frequency response. However, conventional PIT technology needs a strong coupling between the reader and the sensor, requiring the reader to be small to the same extent as the sensors' size. Thus, applying this technology to body-scale sensing systems is challenging. To enable body-scale readout, Twin Meander Coil enhances the sensitivity of PIT technology by dividing the body-scale meander-shaped reader coils into two parts and integrating them so that they support the readout of

Authors' addresses: Ryo Takahashi, The University of Tokyo, Japan, takahashi@akg.t.u-tokyo.ac.jp; Wakako Yukita, The University of Tokyo, Japan, yukita@bhe.t.u-tokyo.ac.jp; Takuya Sasatani, The University of Tokyo, Japan, sasatani@akg.t.u-tokyo.ac.jp; Tomoyuki Yokota, The University of Tokyo, Japan, yokota@ntech.t.u-tokyo.ac.jp; Takao Someya, The University of Tokyo, Japan, someya@ee.t.u-tokyo.ac.jp; Yoshihiro Kawahara, The University of Tokyo, Japan, kawahara@akg.t.u-tokyo.ac.jp.

Permission to make digital or hard copies of all or part of this work for personal or classroom use is granted without fee provided that copies are not made or distributed for profit or commercial advantage and that copies bear this notice and the full citation on the first page. Copyrights for components of this work owned by others than the author(s) must be honored. Abstracting with credit is permitted. To copy otherwise, or republish, or post on servers or to redistribute to lists, requires prior specific permission and/or a fee. Request permissions from permissions@acm.org.

© 2021 Copyright held by the owner/author(s). Publication rights licensed to ACM.

2474-9567/2021/12-ART179 \$15.00

<https://doi.org/10.1145/3494996>

each other. To demonstrate its feasibility, we built a prototype with a knitting machine, evaluated its sensing ability, and demonstrated several applications.

CCS Concepts: • **Human-centered computing** → **Interaction devices**.

Additional Key Words and Phrases: meander, coil, wireless, battery-free, sensing, passive inductive telemetry, knit

ACM Reference Format:

Ryo Takahashi, Wakako Yukita, Takuya Sasatani, Tomoyuki Yokota, Takao Someya, and Yoshihiro Kawahara. 2021. Twin Meander Coil: Sensitive Readout of Battery-free On-body Wireless Sensors Using Body-scale Meander Coils. *Proc. ACM Interact. Mob. Wearable Ubiquitous Technol.* 5, 4, Article 179 (December 2021), 21 pages. <https://doi.org/10.1145/3494996>

1 INTRODUCTION

Advances in materials and electronics have led to the development of various on-body sensors such as fitness trackers, cadence sensors, smart clothing [37, 38], on-skin biosensors [34, 50, 56, 57], and other physiological sensors. Because these sensors can be seamlessly integrated into clothing or accessories, the multiple sensors worn by users can aid in the continuous monitoring of various physiological and environmental signals. Thus, many researchers have investigated the potential applications of such sensors in health monitoring [34], activity recognition [25, 52], and wearable interfaces [11–14, 26, 38, 51].

However, energy-efficient and easy-to-manufacture methods for collecting data from freely placed on-body sensors are missing. The most primitive approach is wiring these sensors [35–37, 52], but the wire disrupts the user’s movements and constrains the sensor positions [29]. Conductive fabrics that connect sensors placed throughout themselves have also been studied, but the electrodes of such fabrics need to be exposed, leading to safety issues and contact failures. Wireless approaches [19, 28, 29, 45] offer safe connections, and textile-based wireless chargers that empower multiple sensor devices have been developed. However, the power transfer efficiency of such textile-based wireless chargers is low (1%–3%), compared with that of standard wireless chargers [44, 54], because textile-based chargers are primarily composed of a highly resistive conductive thread to preserve the flexibility and breathability of clothing [19, 28, 29, 45]. In practice, this low efficiency often requires the sensors to be equipped with bulky batteries for performing continuous sensing tasks. Furthermore, the charger size must be similar to that of the small sensor; if there is a significant size difference, the efficiency significantly decreases [43].

To overcome this challenge, we develop an energy-efficient and unconstrained connection for on-body sensors, as shown in Fig. 1. Our platform is based on wireless sensing technology, namely, highly sensitive passive inductive telemetry (PIT), wherein a body-scale textile-based reader reads out multiple, small, battery-free sensors without powering them up. The textile-based reader coil can be directly knitted into the clothing using Whole Garment and conductive thread. The battery-free sensors can superimpose various sensor values, such as ID, touch, pressure, and rotation, on their frequency responses. In contrast to standard PIT, the highly sensitive PIT enables sensor readout via the weak inductive coupling between the small sensors and large reader. Additionally, the highly sensitive PIT imposes unique challenges when applied to garments because i) the electromagnetic (EM) field generated by the standard coil significantly interacts with the human body, and ii) the inordinate impedance characteristics of the textile-based coil makes the PIT insensitive. Thus, we propose Twin Meander Coil, which enables sensitive readout of on-body sensors via PIT by integrating the two identical meander-shaped reader coils.

2 PASSIVE INDUCTIVE TELEMETRY (PIT)

As shown in Fig. 2(a), PIT employs a passive sensor coil inductively coupled with an external readout coil [24]. The sensing process is as follows. First, the sensor coil passively changes its impedance, *i.e.*, its resonant frequency, $f_0 = 1/2\pi\sqrt{L_{\text{sensor}}C_{\text{sensor}}}$, according to the change of the sensing target (*e.g.*, pressure, temperature). Then, the

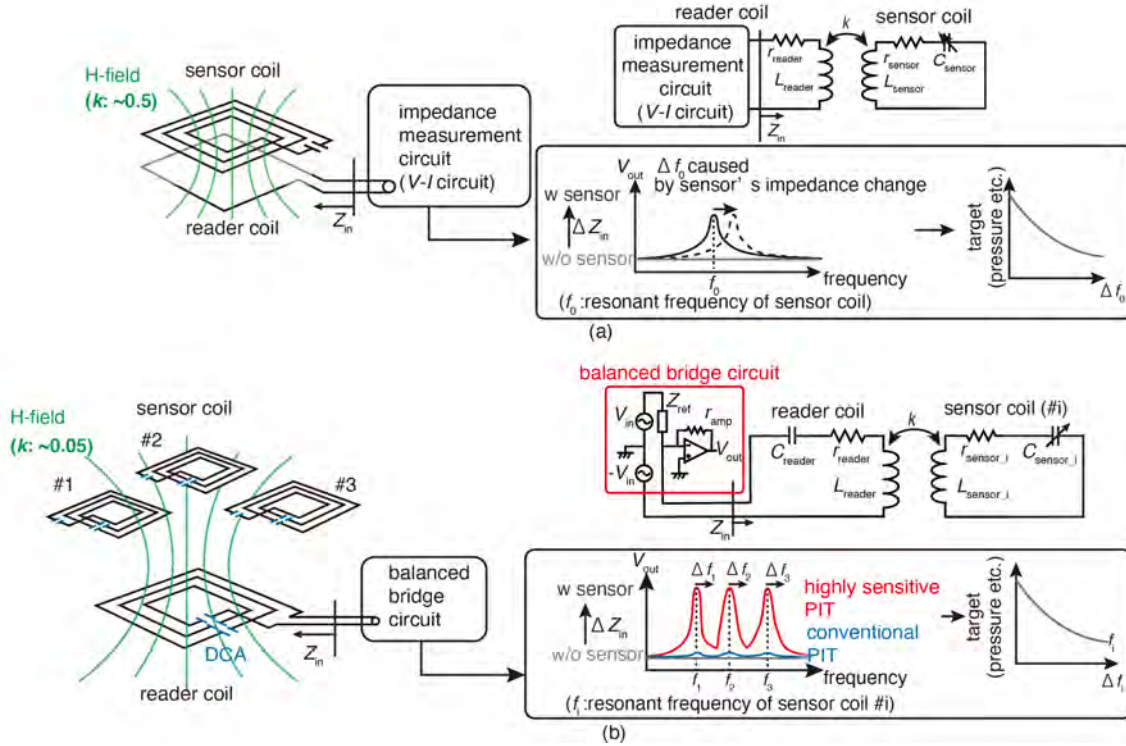


Fig. 2. (a) Overview of conventional PIT with a narrow sensing range, which employs a passive sensor coil inductively coupled with an external readout coil. (b) Overview of highly sensitive PIT, which enables body-scale readout of multiple small sensors using distributed capacitance arrangement (DCA) and balanced bridge circuit [43].

resonant frequency of the sensor can be observed as a peak in the frequency response via the inductively coupled reader coil because the input impedance of the coupled reader coil $Z_{in}(f)$ is known to be a function of sensor impedance as shown in the following:

$$Z_{in}(f) = Z_{reader}(f) + \frac{(2\pi fM)^2}{Z_{sensor}(f)} \quad (1)$$

where Z_{reader} and Z_{sensor} are the impedance of the reader and the sensor, respectively, and $M (= k\sqrt{L_{reader}L_{sensor}})$, k : coupling coefficient, $0 \leq |k| \leq 1$) is the mutual inductance. Note that the peak of Z_{in} appears around f_0 . Finally, the impedance measurement module connected to the reader coil retrieves the sensor value through the peak shift of $Z_{in}(f)$, referred to as Δf_i in Fig. 2.

There are two advantages of PIT when compared to wirelessly powered active sensors. First, PIT only requires a weak magnetic field for readout compared to wireless power solutions [24], and the current of the reader coil can be small (μA – mA), allowing the use of lossy readers composed of conductive threads. Second, the sensor coil need not be equipped with batteries because it is composed of passive components.

However, PIT generally becomes insensitive when the inductive coupling is weak, and this trend imposes challenges when reading out small sensors using large body-scale readers. This occurs because the peak amplitude

of Eq. (1), caused by item $(2\pi f_0 M)^2 / Z_{\text{sensor}}(f_0)$, is positively correlated with M (or k). Thus, when using conventional PIT, the reader size has to be comparable to the sensor size to increase coupling, limiting the applications to small scales, *e.g.*, reading sensors in the pockets of clothes [24].

To this end, TelemetRing proposed a highly sensitive PIT that works in very weakly coupled setups [43], and we aim to develop this technology further to achieve a body-scale PIT that can read out small sensor coils. The highly sensitive PIT involves two technologies: distributed capacitance arrangement (DCA) [9, 43] and a balanced bridge circuit [3], as shown in Fig. 2(b). DCA enhances the equivalent inductance of the coil at high frequencies by inserting multiple series capacitors, which strengthens the inductive coupling ($M = k\sqrt{L_{\text{reader}}L_{\text{sensor}_i}}$). The balanced bridge circuit simplifies the process for impedance matching between the measurement circuit and the reader coil, enabling the detection of the small impedance peaks, as described in § 4.2. Furthermore, multiple sensor coils can be identified by allocating each sensor coil on different frequency bands by adjusting the sensor resonant frequency.

However, highly sensitive PIT imposes two unique challenges when applied to body-scale garments. First, the EM field generated by the body-scale readers interacts with the dielectric human body, making the coupling between the body-scale reader and sensors unstable. Second, the reader coil composed of conductive threads exhibits unique impedance frequency responses (which even change by washing), making impedance matching a challenge.

3 CONTRIBUTION

This work presents Twin Meander Coil, a body-scale PIT system to overcome the above challenges. The two technical features of this work are the following: (i) the proposal of meander-shaped body-scale coils fabricated via ordinary garment manufacture process, and (ii) the integration of the two such meander-shaped coils so that they support the readout of each other. As for (i), unlike standard coils, the meander coil confines the strong EM field near the clothing. Thus, the interaction of the reader with the human body is suppressed while preserving a stable coupling with the sensors near the garment. As for (ii), the two identical meander coils, which have similar impedance characteristics, are integrated into each other's readout circuit as a reference impedance, compensating for the inordinate impedance responses. To examine the feasibility of our design, we built a prototype with a knitting machine and presented several application scenarios.

4 SYSTEM DESIGN

As shown in Fig. 3(a), our system consists of three components: 1) a textile-based reader coil that is composed of two identical meander coils, 2) battery-free sensor coils that have different resonant frequencies and sense various targets such as ID, touch, pressure, and rotation, and 3) an impedance measurement module. The working principle is as follows. First, the multiple sensor coils $\#i$, each of which has different resonant frequency f_i , change their impedance (*i.e.*, C_{sensor_i}) according to the sensing target. By utilizing the highly sensitive PIT, then, the reader coil senses Δf_i of the multiple sensor coils. Finally, the module connected to the reader calculates the sensor value ($\Delta C_{\text{sensor}_i}$) based on both Δf_i and f_i .

4.1 Reader Coil

A standard helix coil wound around the body inevitably interacts with the body via the EM field. Thus, we employ a meander coil, which changes the winding direction from clockwise to counter-clockwise and vice versa in each turn. Flat-shaped meander coils [27, 41] are often used because their zigzag pattern can easily fit into various flat surfaces. In contrast, our work focuses on a cylinder-shaped meander coil. As shown in Fig. 3(b), the meander coil indicates a relatively strong EM field around the clothing while cancelling out the EM field permeating the body. This EM field focused near the clothing is sufficient for the reader to sense the sensors because the sensors

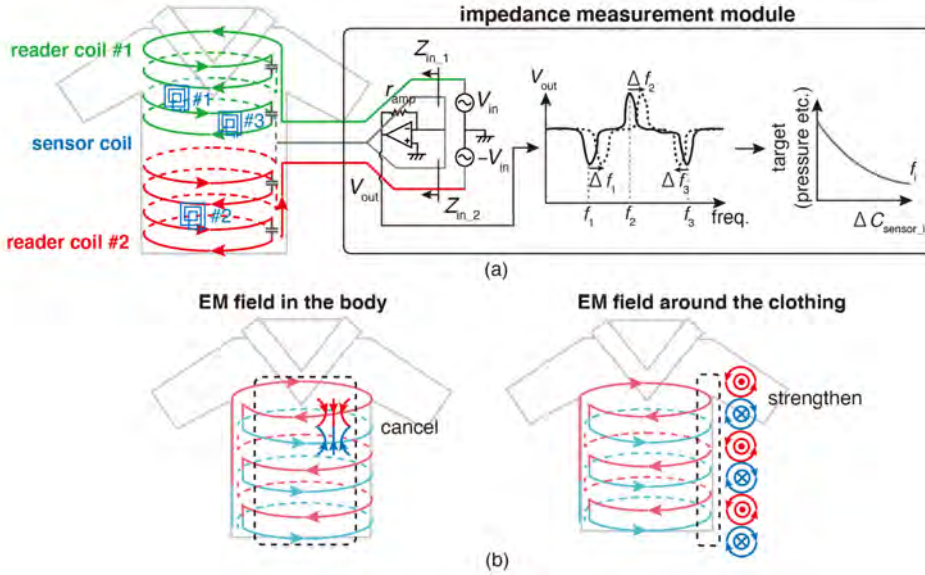


Fig. 3. (a) System overview of Twin Meander Coil, which consists of three components: 1) a textile-based reader coil that is composed of two identical meander coils, 2) battery-free sensor coils that have different resonant frequencies, and 3) an impedance measurement module. (b) Overview of the inductive field generated by meander coil. The meander coil indicates a relatively strong EM field around the clothing while canceling out the EM field permeating the body.

are typically placed on the clothing or the body to detect the physiological signals. Thus, the cylinder-shaped meander coil makes the readout more stable than a standard helix coil.

To demonstrate the feasibility of the cylinder-shaped meander coil, we first simulated the EM field of the proposed meander coil and the standard coil, as shown in Fig. 4(a)-(c). The simulation was conducted using Altair FEKO, an EM simulation software. As shown in Fig. 4(a), we used a cylinder-shaped human model (relative permittivity: 132, conductivity: 0.66 S/m, height: 16 cm, diameter: 26 cm) for simplicity, referring to [8, 22], and a reader coil comprising copper wire (number of turns: 5, wire diameter: 0.5 mm, pitch: 4 cm). Fig. 4(b)(c) show the simulated EM field generated by the two coils (Input power: 1 W, operating frequency: 13.56 MHz); these field distributions indicate that the meander coil suppresses the EM field penetrating the body.

Next, we evaluated the coupling coefficient (k). As shown in Fig. 4(d), we made a 3 cm × 3 cm square PCB sensor coil and two body-scale reader coils (one is a helix and the other is meander-shaped). The body-scale coils were directly integrated into clothing using a knitting machine called Whole Garment (MACH2XS 15S, SHIMA SEIKI), which knits 3D clothing without sewing [1, 33]. Then, we measured the coupling coefficient between the sensor coil and the two reader coils based on the Z -parameters obtained via a vector network analyzer (R&S ZNB20, Rohde & Schwarz). We treated this two-port network as an inductively coupled LC series resonant circuit herein. Fig. 4(e)(f) show the measured coupling coefficient (k) for different sensor positions and distances from the clothing. The position and distance of the sensor coil were varied from 0 cm to 24 cm in steps of 1 cm (position) and from 0 cm to 5 cm in steps of 0.5 cm (distance), respectively. The results show that k of the meander coil becomes stronger than that of the standard coil.

There is an important trade-off between the coupling coefficient (read-out accuracy) and available sensing ranges. When the sensor is placed on positions where k becomes low, the impedance variation of the sensor

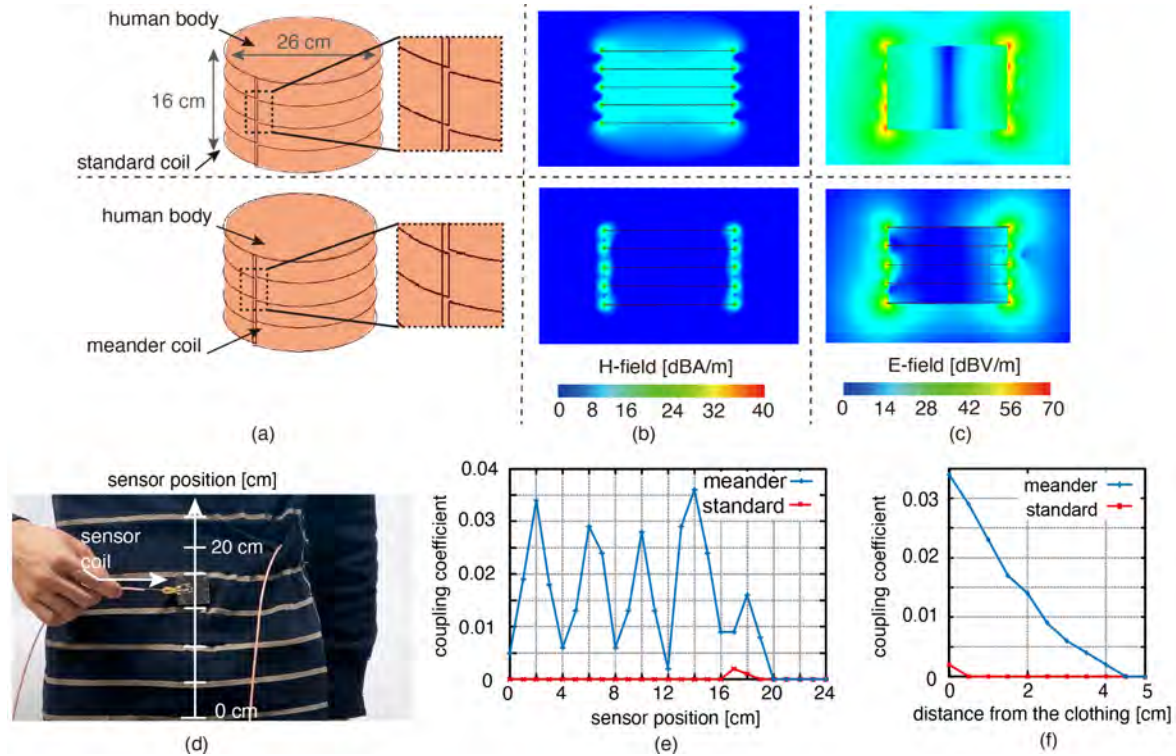


Fig. 4. (a) Simulation model of two kinds of coils and (b)(c) their simulated EM field. These field distributions indicate that the meander coil suppresses the EM field penetrating the body. (d) Experiment setup to measure the coupling coefficient and (e)(f) corresponding results. The results show that k of the meander coil becomes stronger than that of the standard coil.

coil $((2\pi fM)^2/Z_{\text{sensor}}(f))$ is so small that even our highly sensitive readout system cannot detect the frequency peak. Limiting the positions of the sensor coils to where the inductive coupling becomes strong will favor the system's reliability. However, this shrinks the readout range of the system because the areas offering strong inductive coupling are limited. Particularly, when the threshold is set to $(k > 0.02)$, our system can cover about 50% of the entire clothing surface; as this is enough for use in the applications presented in the paper, we decided that this threshold is appropriate. Note that the threshold value of k subsequently affects the frequency range where the frequency peak can be robustly detected, as described in § 7.1.

4.2 Twin Meander Coil

The combination of DCA and the balanced bridge circuit is essential for achieving highly sensitive PIT on clothing. As will be described in Fig. 7(c), DCA can easily be applied to a textile-based reader coil by attaching multiple chip capacitors onto the meander coil. However, the balanced bridge circuit becomes insensitive because it fails to achieve impedance matching over wide frequency ranges when used with the textile-based reader coil.

To understand this difficulty, we first explain the working principle of the balanced bridge circuit shown in Fig. 2(b). The balanced bridge circuit is a variation of the bridge circuit [3], which requires the measured impedance (the reader coil's input impedance herein) to be matched with the reference load to sense small impedance changes. TelemetRing used *LCR* chip components to achieve impedance matching for the reader coil

fabricated on flexible PCBs (*i.e.*, $Z_{\text{ref}} = Z_{\text{reader}}$) over a wide frequency band. When the measurement circuit is impedance-matched, $V_{\text{out}}(f_i)$, the output voltage of the balanced bridge circuit at the resonant frequency of the sensor coil $\#i$ (f_i), can be expressed as follows using Eqn 1:

$$V_{\text{out}}(f_i) = -r_{\text{amp}}I \quad (2)$$

$$= -r_{\text{amp}} \left(\frac{V_{\text{in}}(f_i)}{Z_{\text{ref}}(f_i)} - \frac{V_{\text{in}}(f_i)}{Z_{\text{in}}(f_i)} \right) \quad (3)$$

$$\approx \begin{cases} 0: \text{no sensor } \#i \\ -r_{\text{amp}} \frac{\Delta Z_{\text{in}}(f_i)}{Z_{\text{in}}(f_i)^2} V_{\text{in}}(f_i) : \text{one sensor } \#i \text{ is inductively coupled with reader} \end{cases} \quad (4)$$

where I is the current flowing through r_{amp} , V_{in} is the input voltage, r_{amp} is the gain factor, and $\Delta Z_{\text{in}}(f_i)$ is the very small change of $Z_{\text{in}}(f_i)$ caused by the sensor coil $\#i$. Note that the off-resonant sensor coil $\#j$ ($\neq i$) does not affect the $V_{\text{out}}(f_i)$ because $Z_{\text{sensor}_j}(f_i)$ is very large at f_i . Based on Eqn. 4, TelemetRing can detect the impedance change in the multiple sensor coils by calculating the phase or magnitude spectrum of V_{out} .

However, achieving impedance matching with chip elements for textile-based reader coils over a wide frequency band is challenging. This is because the impedance characteristics of textile coils composing conductive threads significantly differs from those of the *LCR* chip elements. To confirm this, we examined the impedance characteristics of the *LCR* chip elements and the two meander-shaped reader coils. As shown in Fig. 5(a), the two meander-shaped reader coils were fabricated using conductive thread. In addition, the *LCR* chip elements were matched to the reader coil $\#1$ at 13.56 MHz ($L : 2.7 \mu\text{H}$, $C : 50 \text{ pF}$, $R : 61 \Omega$). Fig. 5(b)(c) show the real and imaginary parts of the impedance of both the coil and the *LCR* chip elements ranging from 10 MHz–20 MHz, respectively. The real part of impedance shows significantly different curve between the reader coils and the chip. This is because the stray capacitors in the conductive threads (see Fig. 5(a)) causes the complicated impedance characteristics [16].

To solve this challenge, we need a reference with impedance characteristics similar to that of the textile-based reader coil. Thus, we develop a novel impedance matching method that integrates two identical meander-shaped reader coils into the balanced bridge circuit, as illustrated in Fig. 3. With this method, each reader coil not only works as *reader*, but also functions as *reference* for the other reader coil because the two reader coils $\#i$ ($i = 1, 2$) have almost the same impedance characteristics over a wide frequency band. In addition, the two coils can be placed close to each other because the meander-shaped reader coil confines the EM field only around the wire, unlike the standard coil.

Based on this approach, the output of the balanced bridge circuit, shown in Fig. 3(a), can be expressed as follows:

$$V_{\text{out}}(f_i) = -r_{\text{amp}} \left(\frac{V_{\text{in}}(f_i)}{Z_{\text{in}_1}(f_i)} - \frac{V_{\text{in}}(f_i)}{Z_{\text{in}_2}(f_i)} \right) \quad (5)$$

$$\approx \begin{cases} 0: \text{sensor } \#i \text{ is neither on reader } \#1 \text{ and reader } \#2 \\ r_{\text{amp}} \frac{\Delta Z_{\text{in}_1}(f_i)}{Z_{\text{in}_1}(f_i)^2} V_{\text{in}}(f_i) : \text{sensor } \#i \text{ is on reader } \#1 \\ -r_{\text{amp}} \frac{\Delta Z_{\text{in}_2}(f_i)}{Z_{\text{in}_2}(f_i)^2} V_{\text{in}}(f_i) : \text{sensor } \#i \text{ is on reader } \#2 \end{cases} \quad (6)$$

where $Z_{\text{in}_i} : i = 1, 2$ is the input impedance of the reader coil $\#i$. The two meander coils are separated by 8 cm (= wire space: 4 cm \times 2) to avoid the inductive interference between them. Thus, the sensor coil placed on

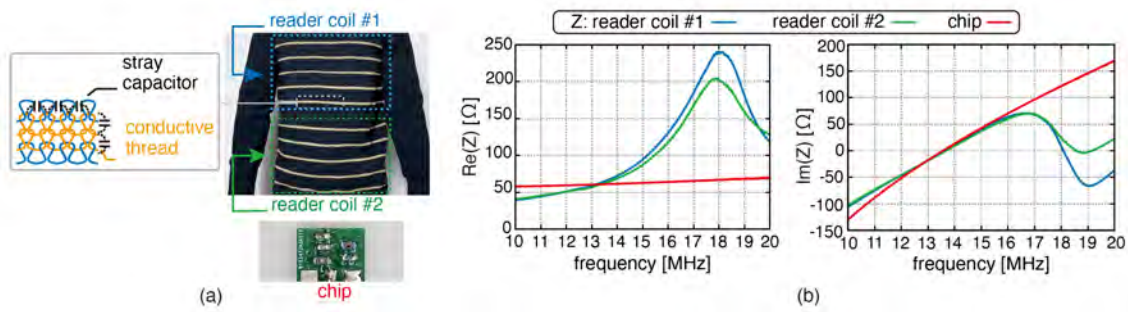


Fig. 5. (a) Overview of two reader coils and LCR chip elements. (b) Impedance characteristics of the two coils and the chip elements. The impedance characteristics of the knitted coils significantly differs from those of the chip elements.

the reader coil $#i$ does not affect the other reader coil $#j$ ($j \neq i$). Note that the output of Eqn. 6 is the same as that of Eqn. 4, although the sign of V_{out} changes depending on which reader the sensor is placed on. In addition, multiple sensor coils $#i$ that have the same resonant frequency f_i cannot be placed on the reader coils because sensor responses imposed on the same frequencies cannot be separated in the current implementation.

Note that even if the number of turns of the two reader coils is different, we can still use this balanced bridge circuit. Considering that the two meander-shaped coils with a size ratio of $\alpha : 1$ satisfy the following relationship: $\alpha Z_{\text{in}_1}(f) = Z_{\text{in}_2}(f)$, the output of the balanced bridge circuit can be modified by tuning the two input voltage ratios to $\alpha : 1$ as follows:

$$V_{\text{out}}(f_i) = -r_{\text{amp}} \left(\frac{\alpha V_{\text{in}}(f_i)}{\alpha Z_{\text{in}_1}(f_i)} - \frac{V_{\text{in}}(f_i)}{Z_{\text{in}_2}(f_i)} \right) \quad (7)$$

The output of Eqn. 7 is similar to that in Eqn. 3.

5 IMPLEMENTATION

Here, we describe the implementation of the three components of Twin Meander Coil: the textile-based reader coil, the battery-free sensor coil, and the impedance measurement module.

5.1 Textile-based Reader Coil

Fig. 6 shows the four prototypes of Twin Meander Coil. Referring to the UNIQLO size table of Japanese men's clothing, we implemented small-, medium-, and large-sized tops. According to the clothing size, we adjusted the number of turns of the reader coil $#i$ ($i=1,2$) for each clothing. Thus, the input voltage ratio of the balanced bridge circuit needs to be tuned according to the number of turns. For example, the input voltage ratio α of Fig. 6(a), (c), (d) is tuned to $\alpha = 1$, whereas that of Fig. 6(b) is tuned to $\alpha = 0.8$, as explained in § 7.

Fig. 7(a)-(c) illustrates the fabrication process of Twin Meander Coil. First, the textile-based reader coil was knitted using Whole Garment (MACH2XS 15S, Shima Seiki), as shown in Fig. 7(a)(b). The reader coil consists of a conductive thread (AGposs, Mitsufuji Corporation) and a non-conductive thread (BabyFit, Asahi Kasei Advance Corporation). To knit the item of clothing with the multiple threads, intarsia (see Fig. 6(a)-(c)) and jacquard techniques (see Fig. 6(d)) were employed, as shown in Fig. 7(d). The jacquard knitting technique can hide the coil pattern inside the clothing, although it takes longer to knit than the intarsia. Then, for DCA, multiple 180 pF–220 pF chip capacitors, soldered on the flexible PCBs, were attached to the coil. Using the multiple chip capacitors, the resonant frequency of the reader coil was tuned at 13.56 MHz, which is one of the ISM bands.



Fig. 6. Four prototypes of our textile-based reader coil knitted using (a)–(c) intarsia technique and (d) jacquard technique.

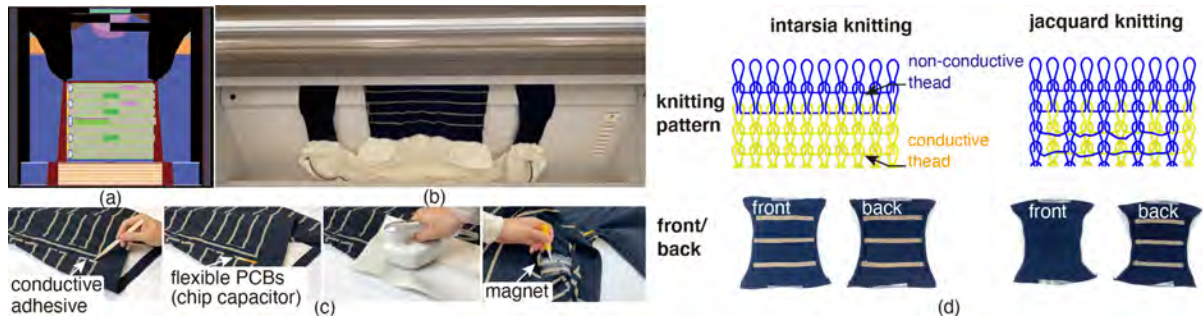


Fig. 7. (a) Knit pattern of Twin Meander Coil. (b)–(d) Fabrication process of our textile-based reader coil. First, Twin Meander Coil is knitted with Whole Garment, and then, the flexible PCBs are attached using conductive adhesive, and finally, three magnets are attached inside the clothing.

To ensure a firm connection between the coil and the flexible PCBs, heat sealing using an Ag (silver) adhesive paste was applied. Finally, using an instant adhesive, three neodymium magnets (ϕ : 5 mm, thickness: 2 mm) were attached inside the clothing, as shown in Fig. 7(c). The magnets are a connector for the impedance measurement module, as described in § 5.3. The inductance (L_{reader}) and resistance (r_{reader}) of the reader coil shown in Fig. 9 are approximately $2.2 \mu\text{H} - 2.7 \mu\text{H}$ and $40 \Omega - 90 \Omega$ ranging from 11 MHz to 16 MHz, respectively.

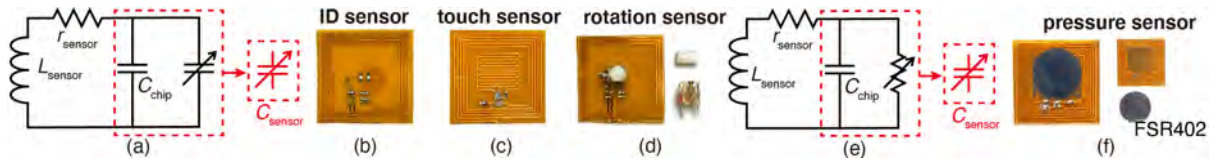


Fig. 8. (a)(e) The circuit diagram of the battery-free sensor coils. Our battery-free sensor coils include (b) ID sensor, (c) touch sensor, (d) rotation sensor, and (f) pressure sensor.



Fig. 9. (a) Overview of our impedance measurement module. The module is connected to the clothing via the magnetic connector. (b) Example of signal processing when five different sensor coils are placed on the clothing. Based on the output values, the PC detects the frequency peaks based on a peak detection algorithm, and then, calculates the peak shift.

5.2 Battery-free Sensor Coil

To date, various types of battery-free sensor coils for PIT have been reported [6, 30, 32, 34, 43]. Here, we implemented the ID, touch, rotation, and pressure sensor coils to demonstrate the feasibility of Twin Meander Coil (see § 6). Fig. 8(a) and Fig. 8(e) show the circuit diagram of Fig. 8(b)–(d) and Fig. 8(f), respectively. Each of these sensors consists of a rectangular coil on flexible PCBs (thickness: 0.1 mm, number of turns: 3 – 5, line width: 0.5 mm, spacing: 0.5 mm) connected to a variable sensing capacitor according to the sensing target. The Q -factor, inductance (L_{sensor}), and resistance (r_{sensor}) of the rectangle coil are approximately 40–70, 0.7 μH –1.2 μH , and 1.2 Ω –1.5 Ω ranging from 11 MHz to 16 MHz, respectively.

To implement the sensing capacitor, we employed a chip capacitor as the ID sensor, two pairs of comb-shaped electrodes (2.2 pF) as the touch sensor, a variable capacitor (BFC280905217: 2 pF – 18 pF) as the rotation sensor, and FSR402 as the pressure sensor. Further, a chip capacitor was added in parallel to the sensing capacitor to tune the resonant frequency of the sensor coil. Note that the frequency bands where the sensor coils can be allocated range from 11 MHz to 16 MHz, based on the result of the impedance-matched frequency band of Twin Meander Coil (see § 7.1). Because the maximum frequency shift among five types of sensor coils is confirmed to be approximately ± 0.5 MHz of the rotation sensor coil, the minimum available number of the sensor coils allocated on the impedance-matched frequency band is 5 ($= 5.0 \text{ MHz}/1.0 \text{ MHz}$). However, the number will increase when using a sensor coil with a small frequency shift such as the ID or pressure sensor coil instead of the rotation sensor coil.

5.3 Impedance Measurement Module

As shown in Fig. 9(a), our impedance measurement module consists of a microcontroller (MCU) with Bluetooth Low Energy (Arduino Nano 33 BLE), DDS (AD9532), RF magnitude and phase detector (AD8302), balanced bridge circuit, 1000 mAh LiPo battery, and a magnetic connector consisting of three neodymium magnets (thickness: 2 mm,

diameter: 5 mm). The DDS transmits a sweep signal ranging from 11 MHz–16 MHz in steps of 25 kHz to the balanced bridge circuit. The bridge circuit was implemented using three wide-band operational amplifiers (OPA356) similar to TelemetRing [43]; the amplifier gain r_{amp} was set to 100 Ω . The output voltage from the balanced bridge circuit was sampled using AD8302 and 12-bit ADC of the MCU in 1 s ($= 5 \text{ ms} \times 200$) cycle, and was converted into a magnitude spectrum. The nRF52840 Bluetooth chip transmits these values to the remote PC at approximately 1 fps. Based on the output values, the PC detects the frequency peak of the output based on the peak detection algorithm available in SciPy¹ (see Fig. 9(b)), and then, calculates the peak shift (Δf_i), or sensor value ($\Delta C_{\text{sensor}_i}$) of each sensor coil. In total, the total power consumption of our impedance measurement module is 0.36 W ($= 3.3 \text{ V} \times 0.11 \text{ A}$). Thus, with the 1000 mAh LiPo battery, the module should be able to work continuously for roughly 9 hours. Although the current implementation using COTS components has a relatively large footprint, they could be integrated into a small IC chip in the future to attain a miniaturized module.

6 APPLICATION

Here, we present some potential applications for Twin Meander Coil. We classified the sensor types based on the resonant frequency of the sensor coil (*i.e.*, 11.56 MHz: the ID sensor coil for the chair, 12.56 MHz: the ID sensor coil for the bed, 13.46 MHz: the rotation sensor coil, 13.66 MHz: the touch sensor coil, 14.56 MHz and 15.56 MHz: the pressure sensor coils). Note that the resonant frequency is allocated within the available frequency band.

6.1 Position Estimation by Tagging the Environment

Unlike previous textile-based wireless sensing systems with narrow readout areas [29, 34, 45], Twin Meander Coil can extend the readout area up to body scale. Thus, it can easily monitor the situation of the user and the related surrounding environments. As an example, we demonstrate the application of user location monitoring at home, as illustrated in Fig. 10(a)(b). By attaching the different ID sensor coils to the various places, Twin Meander Coil can estimate the user location. Here, we attached a 11.56 MHz sensor coil array to the chair and a 12.56 MHz sensor coil array to the bed. The sensor array consists of two similar ID sensor coils placed 2 cm apart. Thus, the body-scale reader can detect the ID sensor coil while avoiding conditions in which both sensor coils fall into null zones where the coupling coefficient is approximately 0 (Fig. 4(e)).

6.2 Posture Monitoring

Unlike the standard on-body sensor equipped with standard wireless communication modules such as BLE or Wi-Fi, Twin Meander Coil enables low-cost and maintenance-free body sensor monitoring. This is because a) the sensor coil is low-cost ($< 1\$$) and battery-free, and b) the reader coil only emits a low-power magnetic field. Based on these advantages, we demonstrate the posture monitoring on the sofa and bed, as shown in Fig. 10(c)–(e). In this application, the two pressure sensor coils were attached on the body directly (see Fig. 10(c)) or inserted into the pocket of the clothing (see Fig. 10(d)(e)). Combining the pressure sensors with the ID sensor coils installed on the sofa or bed, Twin Meander Coil can estimate the user’s specific posture depending on the user’s location. For example, Twin Meander Coil estimates the two kinds of the user situations on the sofa (sitting with one’s back straight or relaxed), as shown in Fig. 10(c), and the two kinds of the user’s sleeping posture on the bed (lying on the back or on one’s side), as shown in Fig. 10(d). In addition, as shown in Fig. 10(d)(e), the user can adjust the arrangement of the sensor coils freely without re-designing the wire pattern of the reader coil; the previous textile-based reader coils require the wire to be re-designed to adjust the placement of the sensor pattern because the reader coil is so small that the readout area is narrow. Although the monitoring based on the current sensor coils supports only simple posture monitoring, the further implementation of heartrate [34],

¹https://docs.scipy.org/doc/scipy/reference/generated/scipy.signal.find_peaks.html

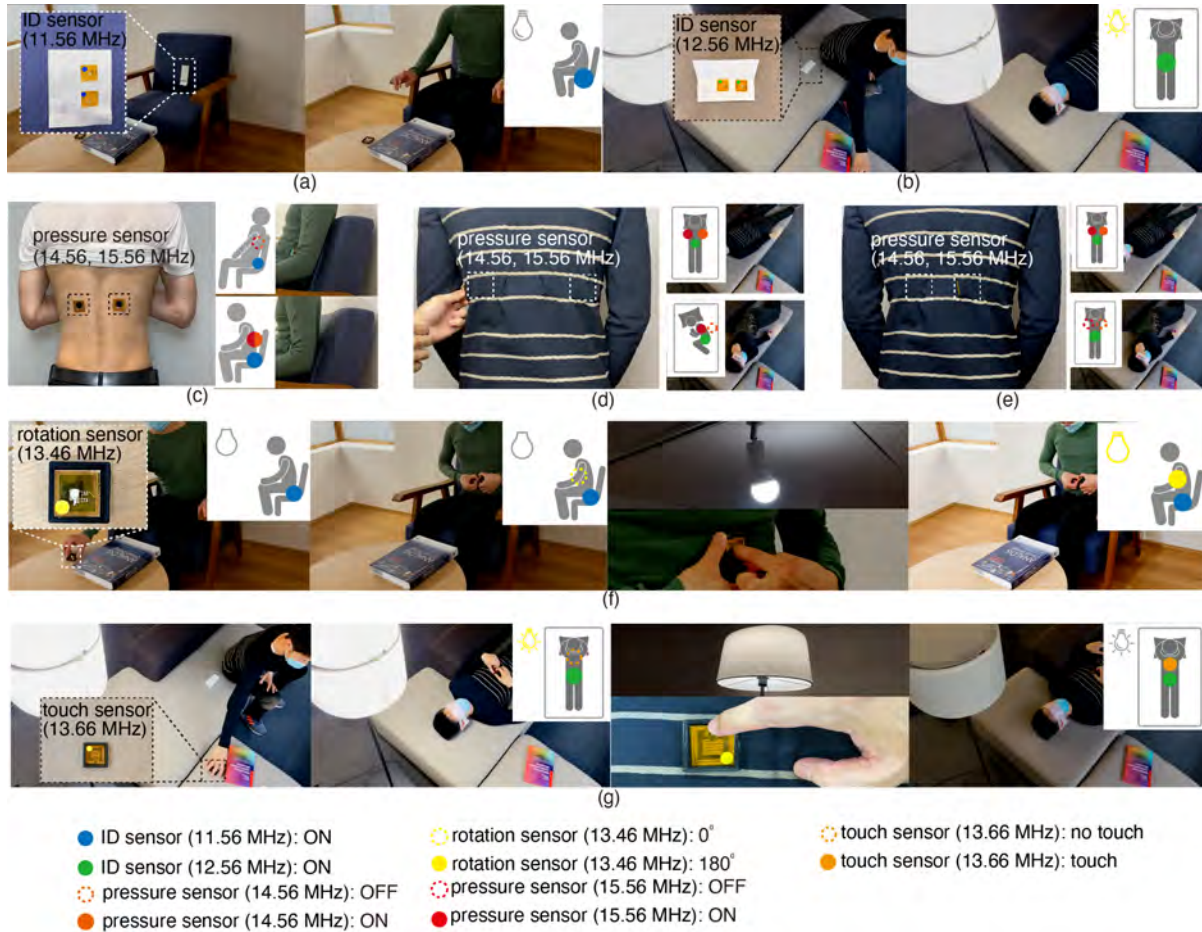


Fig. 10. Application scenarios of Twin Meander Coil: (a)(b) estimation of user's place, (c)-(e) monitoring of user's posture and (f)(g) lightness control with battery-free remote controller.

on-skin temperature [56], or accelerometer [43] sensor coils will enable advanced monitoring, such as personal healthcare or activity recognition.

6.3 Sustainable and Low-cost Remote Controller

Although wired power transfer on clothing needs the sensor to be directly connected with wiring, Twin Meander Coil only requires the sensor to be placed on the clothing. The arrangement avoids wire damage by the electrical connection and enables the wire to be hidden inside the clothing. Thus, the user can repeatedly attach or detach the sensor on the clothing like an accessory. As an example, we present a battery-free remote controller (see Fig. 10(f)(g)). The remote controller includes two types: a brightness controller comprising the rotation sensor coil and an on/off button consisting of the touch sensor coil. Combining the system with the ID sensor coils installed on the sofa or bed, the user can control the nearby light by attaching the remote controller to the clothing.

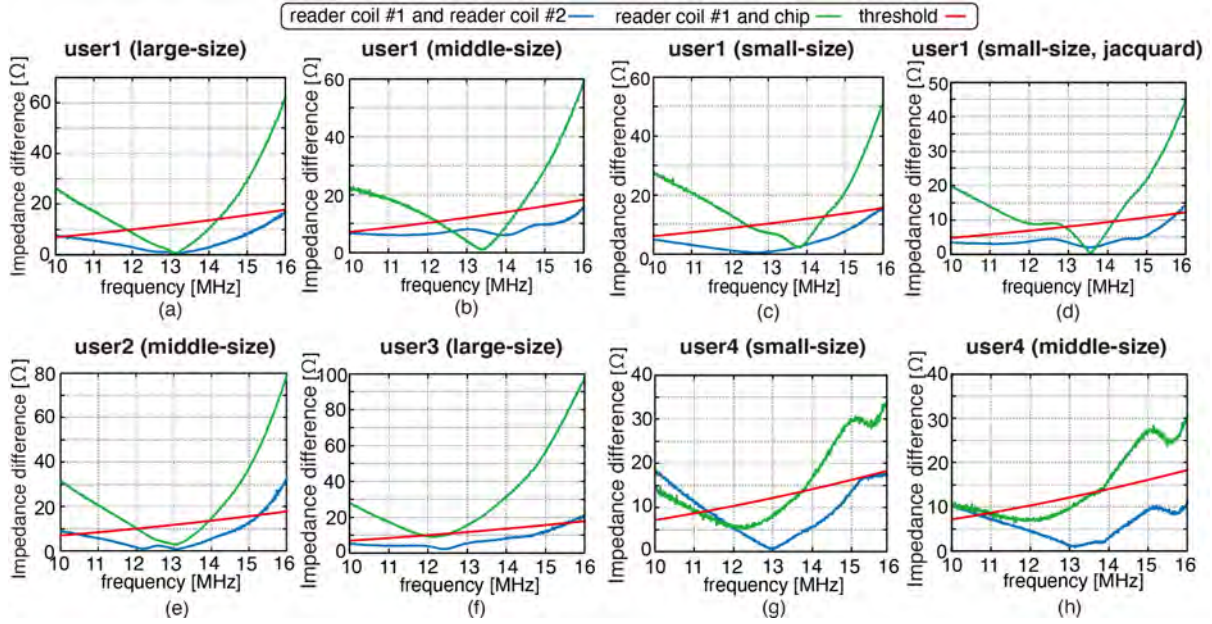


Fig. 11. Impedance difference between the reader coil #1 and #2, or between the reader coil #1 and the chip elements. The available frequency band using the two identical coils is approximately 2 to 8 times wider than that with the chip elements.

Table 1. Resonant frequency of reader coil #1 and available frequency band when being impedance-matched with reader coil #2 or chip elements.

user, clothes' size, knitting method	resonant frequency of reader coil #1	impedance-matched frequency band with reader coil #2	impedance-matched frequency band with chip elements
user1, large-size, intarsia (Fig. 11(a))	13.56 MHz	5.83 MHz	2.39 MHz
user1, middle-size, intarsia (Fig. 11(b))	13.56 MHz	5.98 MHz	2.04 MHz
user1, small-size, intarsia (Fig. 11(c))	13.56 MHz	5.95 MHz	1.98 MHz
user1, small-size, jacquard (Fig. 11(d))	13.56 MHz	5.76 MHz	1.28 MHz
user2, middle-size, intarsia (Fig. 11(e))	13.47 MHz	4.92 MHz	1.92 MHz
user3, large-size, intarsia (Fig. 11(f))	13.33 MHz	5.58 MHz	0.66 MHz
user4, small-size, intarsia (Fig. 11(g))	13.62 MHz	4.79 MHz	2.75 MHz
user4, middle-size, intarsia (Fig. 11(h))	13.89 MHz	5.08 MHz	3.09 MHz

7 EVALUATION

Here, we describe the series of evaluations conducted to confirm the feasibility of Twin Meander Coil.

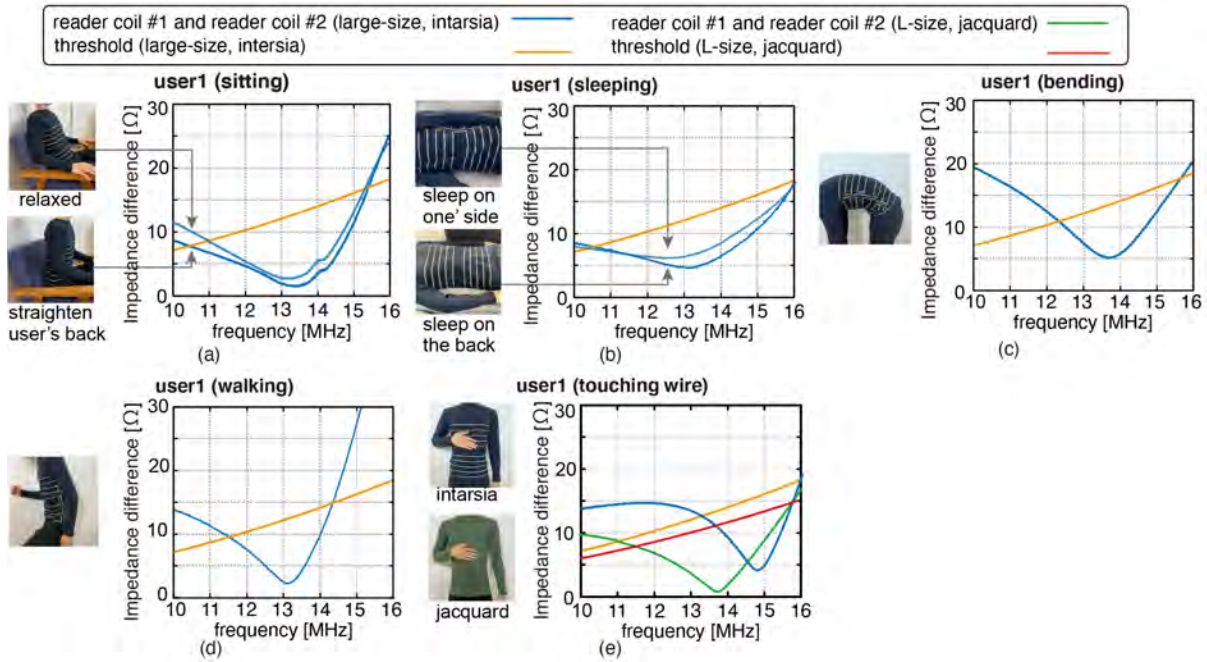


Fig. 12. Impedance difference between the reader coil #1 and #2 in various user's situations: (a) sitting, (b) sleeping, (c) bending, (d) walking actively, and (e) touching the wire on the clothing.

7.1 Available Frequency Band

First, we evaluated the available frequency band of the two impedance matching methods: (i) using two reader coils and (ii) using the *LCR* chip elements along with one reader coil. To calculate the available frequency band, we first examined the impedance difference (i) between the two reader coils i ($i = 1, 2$) of each prototype and (ii) between the *LCR* chip elements and the reader coil #1 for four users (one woman and three men)². The *LCR* chip elements were impedance-matched at 13.56 MHz to the reader coil #1 of the large-sized prototype worn by the user1. Note that the body length of the three users is approximately the same, but their body width is different. We also notice that, in the case of middle size, the impedance of the reader #1 was multiplied by 0.8, because the impedance between the two reader coils with different number of turns can be matched by tuning the input voltage ratio, as described in § 4.2.

Fig. 11 illustrates the result of the impedance difference for the cases (i) and (ii) when the users are standing. Table 1 shows the resonant frequency of the reader #1 and the available frequency band for the cases (i) and (ii). The available frequency band is calculated based on the frequency range for which the impedance difference $\Delta Z_{\text{error}}(f)$ is under the threshold $\Delta Z_{\text{in}}(f) = (2\pi fM)^2/r_{\text{sensor}}$ ($k : 0.02$). The value of k is based on the discussion in § 4.1. When the $\Delta Z_{\text{error}}(f)$ exceeds the sensor variations ($\Delta Z_{\text{in}}(f)$), the frequency peak becomes so small that it is difficult for the module to recognize the peak accurately. Based on the Fig. 11(a)-(h), it was confirmed that the available frequency band for the case (i) is approximately 11 MHz–16 MHz, which is approximately 2 to 8 times wider than that of the case (ii). In addition, the available frequency band for the case (i) is approximately

²user1 is the first author

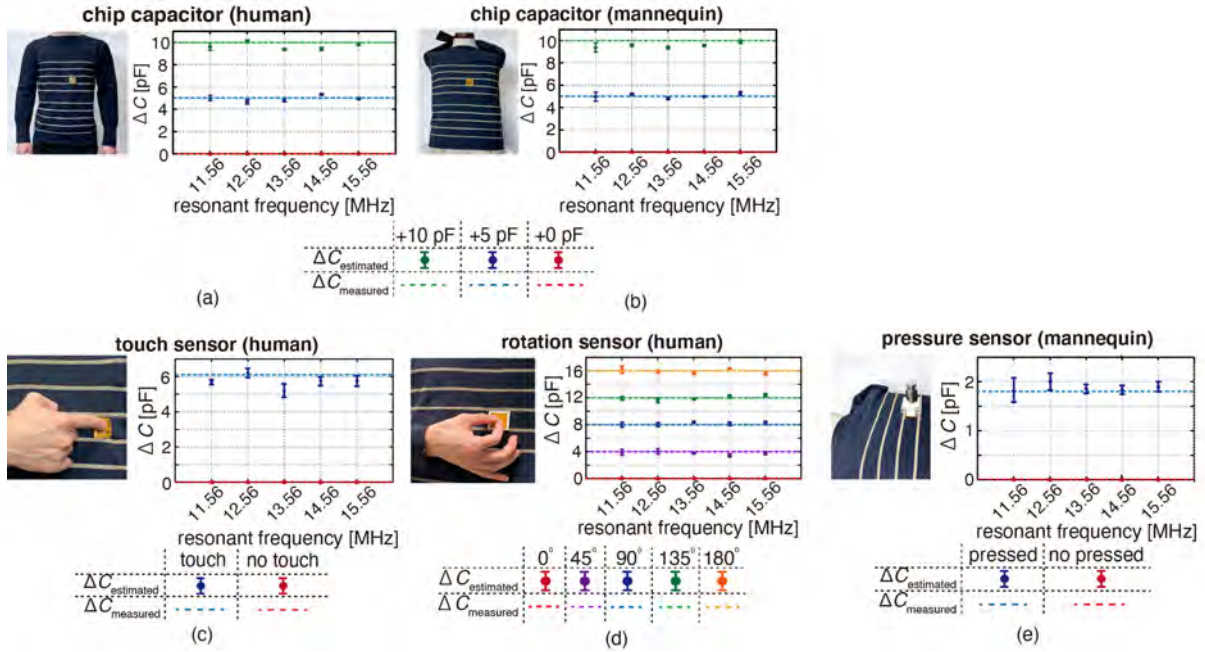


Fig. 13. Sensor value read out via Twin Meander Coil and ground truth of (a)(b) ID sensor, (c) touch sensor, (d) rotation sensor, and (e) pressure sensor. $\Delta C_{\text{estimated}}$ is approximately the same as $\Delta C_{\text{measured}}$, independent of the human or the mannequin.

the same for the other users; this means that Twin Meander Coil can function robustly, although the resonant frequency changes depending on the user's body type.

Fig. 12 illustrates the result of the impedance difference for the cases (i) when the users are sitting, sleeping, bending, and walking. The set of postures shown in Fig. 12 was chosen from the user postures in application scenarios. The available frequency band of Twin Meander Coil is enough wide to detect the sensor coils when the user sits (Fig. 12(a)) and sleeps (Fig. 12(b)) besides they stand. However, the available frequency band becomes significantly narrow when the user bends their hips deeply (Fig. 12(c)) and walks actively (Fig. 12(d)) because of the deformation of the reader coils. As shown in Fig. 12(e), the direct contact of the dielectric hand with the wire also results in the narrow available frequency band. Fortunately, the clothing implemented by jacquard knitting prevents the direct touch with the wire because the wire is hidden inside the clothing, as described in § 5.1.

7.2 Sensor Value

Next, we examined whether Twin Meander Coil could correctly read out the sensor value of the sensor coil. Fig. 13 shows the change in the sensor # i estimated by the module ($\Delta C_{\text{estimated}}$) and the actual change measured by connecting the capacitance part of the sensor coil to an impedance measurement equipment ($\Delta C_{\text{measured}}$). $\Delta C_{\text{estimated}}$ can be estimated as follows considering L_{sensor} and Δf_i of the sensor coil # i :

$$\Delta C_{\text{estimated}} = \frac{1}{\{2\pi(f_i + \Delta f_i)\}^2 L_{\text{sensor}}} - \frac{1}{(2\pi f_i)^2 L_{\text{sensor}}} \quad (8)$$

The five types of our sensor coils are placed at a distance of 10 cm, shown in Fig. 4(d), and the resonant frequency of each sensor coil is tuned at 11.56 MHz, 12.56 MHz, ..., 15.56 MHz.

We began by checking whether $\Delta C_{\text{estimated}}$ is affected by the dielectric human body. To examine this, we compared $\Delta C_{\text{estimated}}$ when the large-sized prototype was worn on a human or styrofoam mannequin. The 5 ID sensor coils were prepared, and further, C_{sensor} of the ID sensor coil was changed by adding a 5 pF or 10 pF chip capacitor in parallel to the fixed chip capacitor of the ID sensor coil. Fig. 13(a)(b) show $\Delta C_{\text{measured}}$ and the average and the standard deviations of $\Delta C_{\text{estimated}}$. It is found that $\Delta C_{\text{estimated}}$ is approximately the same as $\Delta C_{\text{measured}}$, independent of the human or the mannequin.

Then, we measured the sensor value of the three sensors (*i.e.*, touch, rotation, and pressure) when user1 wore the large-sized prototype. Because it is difficult to correctly apply the pressure when the prototype was worn by a human, the pressure value was evaluated by placing the prototype on the mannequin. The measured pressure was 0 kg/cm² and 0.03 kg/cm², and the measured rotation angle was from 0° – 180° in steps of 45°. Fig. 13(c)–(e) show the average and the standard deviations of $\Delta C_{\text{estimated}}$. These results reveal that Twin Meander Coil can discretely but correctly measure the sensor value. To sense the sensor value continuously, one may increase the operating frequency (*e.g.*, from 11 MHz–16 MHz to 24 MHz–29 MHz) and decrease the frequency step size (*e.g.*, from 25 kHz to 10 kHz).

7.3 Washing Durability

Finally, we investigated the washing durability of our clothing, because it must remain protected during regular washing. To examine the durability with daily washing, we washed the three large-sized prototypes (see Fig. 6(a)) with a washing machine, and subsequently, dried the prototypes through air drying. After repeating this process 10 times, we checked whether the prototypes could detect the five ID sensor coils. After 50 washes, one prototype could not detect the ID sensor because the chip capacitor was detached from the flexible PCBs and after 60 washes, the other prototypes stopped working for the same reason. Before this fatal error, the resistance of the two reader coils slightly increased as the clothing was washed³. However, Twin Meander Coil still worked adequately because the two reader coils were impaired similarly, and the impedance characteristics of the two reader coils remained almost the same. These results indicate that Twin Meander Coil is sufficiently durable for daily wash. Note that the durability under all-day wearing, ironing, and repeating wearing/taking-off still needs investigation and is a promising direction for future work.

8 LIMITATIONS AND FUTURE WORK

8.1 Position Detection of Sensor Coils

First, Twin Meander Coil cannot recognize the location of the sensor coil placed on the clothing, although such position detection can increase the range of application scenarios. While previous wearable active sensors can recognize their position by analyzing the IMU data [4, 13] or measuring the time difference from two signal-emitting devices [58]. However, these methods cannot be applied to our system because our sensor coils are completely passive. Because the system can figure out the reader coil coupled with the sensor, one promising approach is to split the meander-shaped coil into many parts, and each reader covers different areas. Thus, we will explore approaches for appropriately separating the meander-shaped reader coils into grids in future work.

8.2 Reading Sensors on Moving Users

Twin Meander Coil is sensitive to the users' motion (*e.g.*, walking), as described in § 7.1. The coil deformation due to the user movement increases the impedance difference between the two reader coils. This limitation requires Twin Meander Coil to conduct the sensor reading under stationary conditions. Fortunately, Twin Meander Coil can mitigate the impedance difference in motion, by tuning the input voltage ratio (α) of the balanced bridge circuit (see § 4.2). For example, the available frequency band shown in Fig. 12 can be increased by tuning the

³The resistance of the two reader coils at 13.56 MHz increased by a factor of approximately 1.2 (61 Ω →75 Ω) after 40 times washing.

input voltage ratio from $\alpha = 1.0$ to $\alpha = 0.8 - 1.2$ in each frequency, to compensate for large impedance differences. Thus, we will integrate a real-time tuning function of the input voltage ratio into the impedance measurement module to enable the sensor reading while in motion.

8.3 Wearability

Although the current prototype knitted by Whole Garment consisted of flexible threads, the attachment of flexible PCBs on the clothing may impair the wearability (*e.g.*, long-term comfort) of the clothing. Thus, we plan to conduct user studies to investigate the wearability of Twin Meander Coil referring to [17].

8.4 Twin Meander Coil for Various Textiles

Finally, we will design Twin Meander Coil for other types of textiles like pants, button-up or zipper-up shirts (*e.g.*, jacket, blouson), bags, blankets, curtains, toys, and we aim to develop a ubiquitous wireless sensing platform for everyday textile. Although the current Twin Meander Coil split into upper and lower parts cannot be applied to the button-up or zipper-up shirts, we will apply Twin Meander Coil to these kinds of clothing by splitting the meander coil into left and right parts. We also plan to enlarge the area of the reader coil up to the sleeve, although the current prototype arranges the reader coils only on the torso of the tops.

9 RELATED WORK

9.1 Energy Harvesting

Energy harvesting, which generates energy from ambient environment or human-generated power, has been widely explored to drive battery-free on-body sensors equipped with wireless communication modules [2, 7, 10, 20, 23, 39, 46, 48]. However, the sensor functions are strictly limited, owing to the lack of the constantly available energy sources and the inefficient energy conversion of the harvester [7]. WISP, which harvests energy from external ultra-high frequency (UHF) RFID signals, can drive accelerometers or temperature sensors without adaptive duty cycling [5]. However, this requires an external UHF RFID reader to be within a relatively short distance (\sim m) from the sensor mainly because the low power transfer efficiency restricts the activation area of the sensor.

9.2 Wired/Wireless Power Transfer

Different from energy harvesting, the textile-based power transmitter can drive the body sensor constantly while the transmitter is active. There are mainly two methods of power transmission: Wired power transfer and wireless power transfer. The former transmits power to the body sensor via electrodes on the clothing [21, 35, 59]. For example, Noda et al. enabled the electric connection by sewing the conductive threads into clothing and designing push-pin-shaped receiver devices [35]. However, safety issues regarding electrical connections remain unsolved as wired power transfer results in the electrodes being exposed to construct electrical connection between sensor and electrodes.

Alternatively, textile-based wireless power transmitters [14, 15, 19, 25, 29, 31, 40, 42, 45, 53, 54] send power to the body sensor without electrical connection. For example, Lin et al. sewn the the small coil array in the clothing using the conductive thread [29] and Tian et al. attached a comb-shaped antenna array to the clothing by cutting the conductive cloth into the comb-shape antenna and gluing it on the clothing [45]. However, wireless charging based on these textile-based transmitter suffers from the low efficiency ($<3\%$) because of the highly resistive conductive thread. Although Worgan et al. embedded the commercially-available rigid transmitter into the clothing [53], such a rigid transmitter significantly impairs the wearability of the clothing. Therefore, we focus on PIT that senses the battery-free body sensor without powering up the sensor. This allows us to design the reader coil using the conductive thread.

9.3 Other Textile-based Wireless Sensing

Similar to Twin Meander Coil, wireless sensing methods on textile have been explored in HCI: EM sensing [55], capacitive sensing [38, 48], and inductive sensing [18, 47, 49]. According to the type of the sensing, each of the previous works enables to recognize the type of gesture input in the air, non-metallic or metallic object, touch gesture, and NFC tag. To implement a textile-based readout system, most works have embedded circuit patterns into clothing by sewing conductive threads because this method is easily available to novices. However, it takes a lot of time and labor to sew a body-scale circuit pattern onto the clothing. Thus, the methods of fabricating the body-scale readout systems based on knitting [1] and weaving [38] have gained attention. Following the trend of the previous approaches, Twin Meander Coil also employs a knitting machine to implement the body-scale meander-shaped coils on the clothing.

10 CONCLUSION

This paper proposed Twin Meander Coil, a clothing-scale wireless sensing platform that supports data collection of multiple battery-free wearable sensors. To detect the small sensors weakly coupled with the large reader, the proposed platform employs both the highly sensitive PIT and the two identical meander coils. A critical benefit of our technology is that it is developed using standard textile manufacturing facilities. Thus, it could be seamlessly integrated into various textile products and enhance the deployment of sustainable wearable sensor systems in the real world.

ACKNOWLEDGMENTS

This work was supported by JST ERATO, Japan under Grant No.: JPMJER1501 and JST ACCEL, Japan under Grant No.: JPMJMI17F1. The authors would like to thank Takashi Ikeuchi for his help of our implementation. The authors would also like to thank the anonymous reviewers for their valuable comments.

REFERENCES

- [1] Lea Albaugh, Scott Hudson, and Lining Yao. 2019. Digital Fabrication of Soft Actuated Objects by Machine Knitting. In *Extended Abstracts of the 2019 CHI Conference on Human Factors in Computing Systems*. ACM, New York, NY, USA, 1–4. <https://doi.org/10.1145/3290607.3313270>
- [2] Walter Bacharowski. 2005. Energy scavenging for remote sensors. *Electronic Design* 53, 28 (2005).
- [3] Larry K Baxter. 1997. Capacitive sensors. *Design and Applications* (1997).
- [4] Hamidreza Bayati, José Del R. Millán, and Ricardo Chavarriaga. 2011. Unsupervised adaptation to on-body sensor displacement in acceleration-based activity recognition. *Proceedings - International Symposium on Wearable Computers, ISWC* (2011), 71–78. <https://doi.org/10.1109/ISWC.2011.11>
- [5] Michael Buettner, Richa Prasad, Alanson Sample, Daniel Yeager, Ben Greenstein, Joshua R Smith, and David Wetherall. 2008. RFID sensor networks with the intel WISP. In *Proceedings of the 6th ACM conference on Embedded network sensor systems - SenSys '08*. ACM Press, New York, New York, USA, 393. <https://doi.org/10.1145/1460412.1460468>
- [6] Yi Chiu, Hao Chiao Hong, and Po Chih Wu. 2013. Development and characterization of a CMOS-MEMS accelerometer with differential lc-tank oscillators. *Journal of Microelectromechanical Systems* 22, 6 (2013), 1285–1295. <https://doi.org/10.1109/JMEMS.2013.2282419>
- [7] Yung Wey Chong, Widad Ismail, Kwangman Ko, and Chen Yi Lee. 2019. Energy Harvesting for Wearable Devices: A Review. *IEEE Sensors Journal* 19, 20 (2019), 9047–9062. <https://doi.org/10.1109/JSEN.2019.2925638>
- [8] Andreas Christ, Mark G. Douglas, John M. Roman, Emily B. Cooper, Alanson P. Sample, Benjamin H. Waters, Joshua R. Smith, and Niels Kuster. 2013. Evaluation of wireless resonant power transfer systems with human electromagnetic exposure limits. *IEEE Transactions on Electromagnetic Compatibility* 55, 2 (2013), 265–274. <https://doi.org/10.1109/TEMC.2012.2219870>
- [9] Bruce Cook and IJ Lowe. 1982. A large-inductance, high-frequency, high-Q, series-tuned coil for NMR. *Journal of Magnetic Resonance* (1969) 49, 2 (9 1982), 346–349. [https://doi.org/10.1016/0022-2364\(82\)90200-1](https://doi.org/10.1016/0022-2364(82)90200-1)
- [10] Jasper de Winkel, Vito Kortbeek, Josiah Hester, and Przemysław Pawelczak. 2020. Battery-Free Game Boy. *Proceedings of the ACM on Interactive, Mobile, Wearable and Ubiquitous Technologies* 4, 3 (9 2020), 1–34. <https://doi.org/10.1145/3411839>
- [11] Artem Dementyev, Tomás Vega Gálvez, and Alex Olwal. 2019. SensorSnaps: Integrating wireless sensor nodes into fabric snap fasteners for textile interfaces. *UIST 2019 - Proceedings of the 32nd Annual ACM Symposium on User Interface Software and Technology* (2019),

- 17–28. <https://doi.org/10.1145/3332165.3347913>
- [12] Artem Dementyev, Javier Hernandez, Inrak Choi, Sean Follmer, and Joseph Paradiso. 2018. Epidermal Robots. *Proceedings of the ACM on Interactive, Mobile, Wearable and Ubiquitous Technologies* 2, 3 (2018), 1–22. <https://doi.org/10.1145/3264912>
- [13] Artem Dementyev, Hsin Liu Cindy Kao, Inrak Choi, Deborah Ajilo, Maggie Xu, Joseph A. Paradiso, Chris Schmandt, and Sean Follmer. 2016. Rovables: Miniature on-body robots as mobile wearables. *UIST 2016 - Proceedings of the 29th Annual Symposium on User Interface Software and Technology* (2016), 111–120. <https://doi.org/10.1145/2984511.2984531>
- [14] Christine Dierk, Molly Jane Pearce Nicholas, and Eric Paulos. 2018. AlterWear: Battery-free wearable displays for opportunistic interactions. *Conference on Human Factors in Computing Systems - Proceedings 2018-April* (2018), 1–11. <https://doi.org/10.1145/3173574.3173794>
- [15] Christine Dierk, Tomás Vega Gálvez, and Eric Paulos. 2017. AlterNail. In *Proceedings of the 2017 CHI Conference on Human Factors in Computing Systems*. ACM, New York, NY, USA, 6754–6759. <https://doi.org/10.1145/3025453.3025924>
- [16] Kristel Fobelets, Kris Thielemans, Abhinaya Mathivanan, and Christos Papavassiliou. 2019. Characterization of Knitted Coils for e-Textiles. *IEEE Sensors Journal* 19, 18 (2019), 7835–7840. <https://doi.org/10.1109/JSEN.2019.2917542>
- [17] Francine Gemperle, Chris Kasabach, John Stivoric, Malcolm Bauer, and Richard Martin. 1998. Design for wearability. *International Symposium on Wearable Computers, Digest of Papers 1998-October* (1998), 116–122. <https://doi.org/10.1109/ISWC.1998.729537>
- [18] Jun Gong, Yu Wu, Lei Yan, Teddy Seyed, and Xing-dong Yang. 2019. Tessutivo. In *Proceedings of the 32nd Annual ACM Symposium on User Interface Software and Technology*. ACM, New York, NY, USA, 29–41. <https://doi.org/10.1145/3332165.3347897>
- [19] Neil J. Grabham, Yi Li, Lindsay R. Clare, Bernard H. Stark, and Stephen P. Beeby. 2018. Fabrication Techniques for Manufacturing Flexible Coils on Textiles for Inductive Power Transfer. *IEEE Sensors Journal* 18, 6 (2018), 2599–2606. <https://doi.org/10.1109/JSEN.2018.2796138>
- [20] Tobias Grosse-Puppenthal, Steve Hodges, Nicholas Chen, John Helmes, Stuart Taylor, James Scott, Josh Fromm, and David Sweeney. 2016. Exploring the Design Space for Energy-Harvesting Situated Displays. In *Proceedings of the 29th Annual Symposium on User Interface Software and Technology*. ACM, New York, NY, USA, 41–48. <https://doi.org/10.1145/2984511.2984513>
- [21] C. K. Harnett. 2017. Tobiko. (2017), 2024–2028. <https://doi.org/10.1145/3025453.3025504>
- [22] Akimasa Hirata, Fumihiro Ito, and Ilkka Laakso. 2013. Confirmation of quasi-static approximation in SAR evaluation for a wireless power transfer system. *Physics in Medicine and Biology* 58, 17 (2013). <https://doi.org/10.1088/0031-9155/58/17/N241>
- [23] Tsung Hsing Hsu, Supone Manakasettharn, J. Ashley Taylor, and Tom Krupenkin. 2015. Bubbler: A Novel Ultra-High Power Density Energy Harvesting Method Based on Reverse Electrowetting. *Scientific Reports* 5 (2015), 1–13. <https://doi.org/10.1038/srep16537>
- [24] Qing An Huang, Lei Dong, and Li Feng Wang. 2016. LC Passive Wireless Sensors Toward a Wireless Sensing Platform: Status, Prospects, and Challenges. *Journal of Microelectromechanical Systems* 25, 5 (2016), 822–841. <https://doi.org/10.1109/JMEMS.2016.2602298>
- [25] Ali Kiaghadi, Morgan Baima, Jeremy Gummeson, Trisha Andrew, and Deepak Ganesan. 2018. Fabric as a Sensor: Towards unobtrusive sensing of human behavior with triboelectric textiles. *SenSys 2018 - Proceedings of the 16th Conference on Embedded Networked Sensor Systems* (2018), 199–210. <https://doi.org/10.1145/3274783.3274845>
- [26] Ali Kiaghadi, Seyedeh Zohreh Homayounfar, Jeremy Gummeson, Trisha Andrew, and Deepak Ganesan. 2019. Phyjama. *Proceedings of the ACM on Interactive, Mobile, Wearable and Ubiquitous Technologies* 3, 3 (2019), 1–29. <https://doi.org/10.1145/3351247>
- [27] Eun S. Lee, Jin S. Choi, Ho S. Son, Seung H. Han, and Chun T. Rim. 2017. Six Degrees of Freedom Wide-Range Ubiquitous IPT for IoT by DQ Magnetic Field. *IEEE Transactions on Power Electronics* 32, 11 (2017), 8258–8276. <https://doi.org/10.1109/TPEL.2017.2691063>
- [28] Yi Li, Neil Grabham, Russel Torah, John Tudor, and Steve Beeby. 2018. Textile-Based Flexible Coils for Wireless Inductive Power Transmission. *Applied Sciences* 8, 6 (2018), 912. <https://doi.org/10.3390/app8060912>
- [29] Rongzhou Lin, Han Joon Kim, Sippanat Achavananthadith, Selman A. Kurt, Shawn C.C. Tan, Haicheng Yao, Benjamin C.K. Tee, Jason K.W. Lee, and John S. Ho. 2020. Wireless battery-free body sensor networks using near-field-enabled clothing. *Nature Communications* 11, 1 (2020), 1–10. <https://doi.org/10.1038/s41467-020-14311-2>
- [30] Manu S. Mannoor, Hu Tao, Jefferson D. Clayton, Amartya Sengupta, David L. Kaplan, Rajesh R. Naik, Naveen Verma, Fiorenzo G. Omenetto, and Michael C. McAlpine. 2012. Graphene-based wireless bacteria detection on tooth enamel. *Nature Communications* 3 (2012). <https://doi.org/10.1038/ncomms1767>
- [31] Noor Mohammed, Rui Wang, Robert W Jackson, Yeonsik Noh, Jeremy Gummeson, and Sunghoon Ivan Lee. 2021. ShaZam. *Proceedings of the ACM on Interactive, Mobile, Wearable and Ubiquitous Technologies* 5, 2 (6 2021), 1–25. <https://doi.org/10.1145/3463505>
- [32] M. Nabipoor and B. Y. Majlis. 2006. A new passive telemetry LC pressure and temperature sensor optimized for TPMS. *Journal of Physics: Conference Series* 34, 1 (2006), 770–775. <https://doi.org/10.1088/1742-6596/34/1/127>
- [33] Vidya Narayanan, Kui Wu, Cem Yuksel, and James McCann. 2019. Visual knitting machine programming. *ACM Transactions on Graphics* 38, 4 (2019). <https://doi.org/10.1145/3306346.3322995>
- [34] Simiao Niu, Naaji Matsuhisa, Levent Beker, Jinxing Li, Sihong Wang, Jiechen Wang, Yuanwen Jiang, Xuzhou Yan, Youngjun Yun, William Burnett, Ada S. Y. Poon, Jeffery B.-H. Tok, Xiaodong Chen, and Zhenan Bao. 2019. A wireless body area sensor network based on stretchable passive tags. *Nature Electronics* 2, 8 (2019), 361–368. <https://doi.org/10.1038/s41928-019-0286-2>
- [35] Akihito Noda and Hiroyuki Shinoda. 2017. Frequency-division-multiplexed signal and power transfer for wearable devices networked via conductive embroideries on a cloth. *IEEE MTT-S International Microwave Symposium Digest* (2017), 537–540. <https://doi.org/10.1109/>

- MWSYM.2017.8058619
- [36] Akihito Noda and Hiroyuki Shinoda. 2019. Inter-IC for Wearables (I2We): Power and Data Transfer over Double-Sided Conductive Textile. *IEEE Transactions on Biomedical Circuits and Systems* 13, 1 (2019), 80–90. <https://doi.org/10.1109/TBCAS.2018.2881219>
 - [37] E. Rehmi Post and Margaret Orth. 1997. Smart fabric, or ‘wearable clothing’. *International Symposium on Wearable Computers, Digest of Papers* (1997), 167–168. <https://doi.org/10.1109/iswc.1997.629937>
 - [38] Ivan Poupyrev, Nan-Wei Gong, Shiho Fukuhara, Mustafa Emre Karagozler, Carsten Schwesig, and Karen E. Robinson. 2016. Project Jacquard: Interactive Digital Textiles at Scale. In *Proceedings of the 2016 CHI Conference on Human Factors in Computing Systems*. ACM, New York, NY, USA, 4216–4227. <https://doi.org/10.1145/2858036.2858176>
 - [39] Vaishnavi Ranganathan, Sidhant Gupta, Jonathan Lester, Joshua R. Smith, and Desney Tan. 2018. RF Bandaid. *Proceedings of the ACM on Interactive, Mobile, Wearable and Ubiquitous Technologies* 2, 2 (7 2018), 1–21. <https://doi.org/10.1145/3214282>
 - [40] Alanson P. Sample, Daniel J. Yeager, Pauline S. Powledge, Alexander V. Mamishev, and Joshua R. Smith. 2008. Design of an RFID-based battery-free programmable sensing platform. *IEEE Transactions on Instrumentation and Measurement* 57, 11 (2008), 2608–2615. <https://doi.org/10.1109/TIM.2008.925019>
 - [41] F. Sato, H. Matsuki, S. Kikuchi, T. Seto, T. Satoh, H. Osada, and K. Seki. 1998. A new meander type contactless power transmission system - Active excitation with a characteristics of coil shape. *IEEE Transactions on Magnetics* 34, 4 PART 1 (1998), 2066–2068. <https://doi.org/10.1109/20.706797>
 - [42] Rishi Shukla, Neev Kiran, Rui Wang, Jeremy Gummeson, and Sunghoon Ivan Lee. 2019. SkinnyPower: Enabling batteryless wearable sensors via intra-body power transfer. *SenSys 2019 - Proceedings of the 17th Conference on Embedded Networked Sensor Systems* (2019), 68–82. <https://doi.org/10.1145/3356250.3360034>
 - [43] Ryo Takahashi, Masaaki Fukumoto, Changyo Han, Takuya Sasatani, Yoshiaki Narusue, and Yoshihiro Kawahara. 2020. TelemetRing: A Batteryless and Wireless Ring-shaped Keyboard using Passive Inductive Telemetry. In *Proceedings of the 33rd Annual ACM Symposium on User Interface Software and Technology*. ACM, New York, NY, USA, 1161–1168. <https://doi.org/10.1145/3379337.3415873>
 - [44] Ryo Takahashi, Takuya Sasatani, Fuminori Okuya, Yoshiaki Narusue, and Yoshihiro Kawahara. 2018. A Cutable Wireless Power Transfer Sheet. *Proceedings of the ACM on Interactive, Mobile, Wearable and Ubiquitous Technologies* 2, 4 (2018), 1–25. <https://doi.org/10.1145/3287068>
 - [45] Xi Tian, Pui Mun Lee, Yu Jun Tan, Tina L.Y. Wu, Haicheng Yao, Mengying Zhang, Zhipeng Li, Kian Ann Ng, Benjamin C.K. Tee, and John S. Ho. 2019. Wireless body sensor networks based on metamaterial textiles. *Nature Electronics* 2, 6 (2019), 243–251. <https://doi.org/10.1038/s41928-019-0257-7>
 - [46] Deepak Vasisht, Guo Zhang, Omid Abari, Hsiao-Ming Lu, Jacob Flanz, and Dina Katabi. 2018. In-body backscatter communication and localization. In *Proceedings of the 2018 Conference of the ACM Special Interest Group on Data Communication*. ACM, New York, NY, USA, 132–146. <https://doi.org/10.1145/3230543.3230565>
 - [47] Nicolas Villar, Daniel Cletheroe, Greg Saul, Christian Holz, Tim Regan, Oscar Salandin, Misha Sra, Hui-Shyong Yeo, William Field, and Haiyan Zhang. 2018. *Project Zanzibar: A Portable and Flexible Tangible Interaction Platform*. Association for Computing Machinery, New York, NY, USA, 1–13. <https://doi.org/10.1145/3173574.3174089>
 - [48] Anandghan Waghmare, Qiuyue Xue, Dingtian Zhang, Yuhui Zhao, Shivan Mittal, Nivedita Arora, Ceara Byrne, Thad Starner, and Gregory Abowd. 2020. UbiquiTouch: Self Sustaining Ubiquitous Touch Interfaces. *Proceedings of the ACM on Interactive, Mobile, Wearable and Ubiquitous Technologies* 4, 1 (2020), 1–22. <https://doi.org/10.1145/3380989>
 - [49] Jingxian Wang, Junbo Zhang, Ke Li, Chengfeng Pan, Carmel Majidi, and Swarun Kumar. 2021. Locating Everyday Objects using NFC Textiles. (2021), 15–30. <https://doi.org/10.1145/3412382.3458254>
 - [50] Yan Wang, Sunghoon Lee, Tomoyuki Yokota, Haoyang Wang, Zhi Jiang, Jiabin Wang, Mari Koizumi, and Takao Someya. 2020. A durable nanomesh on-skin strain gauge for natural skin motion monitoring with minimum mechanical constraints. *Science Advances* 6, 33 (2020), 1–10. <https://doi.org/10.1126/sciadv.abb7043>
 - [51] Irmandy Wicaksono, Juliana Cherston, and Joseph A Paradiso. 2021. Electronic Textile Gaia: Ubiquitous Computational Substrates Across Geometric Scales. *IEEE Pervasive Computing* 20, 3 (7 2021), 18–29. <https://doi.org/10.1109/MPRV.2021.3078107>
 - [52] Irmandy Wicaksono, Carson I. Tucker, Tao Sun, Cesar A. Guerrero, Clare Liu, Wesley M. Woo, Eric J. Pence, and Canan Dagdeviren. 2020. A tailored, electronic textile conformable suit for large-scale spatiotemporal physiological sensing in vivo. *npj Flexible Electronics* 4, 1 (2020). <https://doi.org/10.1038/s41528-020-0068-y>
 - [53] Paul Worgan and Mike Fraser. 2016. Garment level power distribution for wearables using inductive power transfer. *Proceedings - 2016 9th International Conference on Human System Interactions, HSI 2016* (2016), 277–283. <https://doi.org/10.1109/HSI.2016.7529644>
 - [54] Paul Worgan, Jarrod Knibbe, Mike Fraser, and Diego Martinez Plasencia. 2016. PowerShake: Power Transfer interactions for mobile devices. *Conference on Human Factors in Computing Systems - Proceedings* (2016), 4734–4745. <https://doi.org/10.1145/2858036.2858569>
 - [55] Te Yen Wu, Shutong Qi, Junchi Chen, Mu Jie Shang, Jun Gong, Teddy Seyed, and Xing Dong Yang. 2020. Fabriccio: Touchless Gestural Input on Interactive Fabrics. *Conference on Human Factors in Computing Systems - Proceedings Figure 1* (2020), 1–14. <https://doi.org/10.1145/3313831.3376681>

- [56] Tomoyuki Yokota, Yusuke Inoue, Yuki Terakawa, Jonathan Reeder, Martin Kaltenbrunner, Taylor Ware, Kejia Yang, Kunihiko Mabuchi, Tomohiro Murakawa, Masaki Sekino, Walter Voit, Tsuyoshi Sekitani, and Takao Someya. 2015. Ultraflexible, large-area, physiological temperature sensors for multipoint measurements. *Proceedings of the National Academy of Sciences* 112, 47 (11 2015), 14533–14538. <https://doi.org/10.1073/pnas.1515650112>
- [57] Tomoyuki Yokota, Takashi Nakamura, Hirofumi Kato, Marina Mochizuki, Masahiro Tada, Makoto Uchida, Sunghoon Lee, Mari Koizumi, Wakako Yukita, Akio Takimoto, and Takao Someya. 2020. A conformable imager for biometric authentication and vital sign measurement. *Nature Electronics* 3, 2 (2020), 113–121. <https://doi.org/10.1038/s41928-019-0354-7>
- [58] Kazuki Yoshida and Kazuya Muraio. 2019. Estimating load positions of wearable devices based on difference in pulse wave arrival time. *Proceedings - International Symposium on Wearable Computers, ISWC (2019)*, 234–243. <https://doi.org/10.1145/3341163.3347743>
- [59] Tengxiang Zhang, Xin Yi, Chun Yu, Yuntao Wang, Nicholas Becker, and Yuanchun Shi. 2017. TouchPower. *Proceedings of the ACM on Interactive, Mobile, Wearable and Ubiquitous Technologies* 1, 3 (9 2017), 1–20. <https://doi.org/10.1145/3130986>